JOURNAL OF SPACECRAFT AND ROCKETS
Vol. 37, No. 6, November–December 2000

Reassessment of Effect of Dust Erosion on Heatshield of Mars Entry Vehicle

Grant Palmer* and Y.-K. Chen†
NASA Ames Research Center, Moffett Field, California 94035
and
Periklis Papadopoulos‡ and Michael Tauber§
Eloret Corporation, Sunnyvale, California 94087

A computation is performed to assess the surface erosion due to dust particle impact for the Mars 2001 Lander vehicle. A previous study on a Mars aerocapture vehicle indicated that a significant amount of dust erosion would take place. The present calculation uses a three-dimensional Navier–Stokes flow solver and a more sophisticated atmospheric dust model to provide inputs for the dust erosion algorithm. The new dust model predicts a lower mass mixing ratio and a smaller average dust particle size than previous models. The computed surface erosion on the Mars 2001 Lander vehicle is found to be negligible.

Nomenclature

C_D	=	drag coefficient
c	=	mass fraction
D	=	diffusion coefficient, m^2/s
d	=	diameter, m
h	=	specific enthalpy, J/K
M_r	=	mass mixing ratio
q	=	heat flux, W/m^2
r	=	radius, m
s	=	distance along trajectory, m
t	=	time, s
V	=	velocity, m/s
y	=	crater depth, m
y_{total}	=	total surface erosion, m
ε	=	emissivity
η	=	direction normal to vehicle surface
κ	=	thermal conductivity, J/m · s · K
ρ	=	density, kg/m^3
σ	=	Stefan–Boltzmann constant

Subscripts

c	=	crater
p	=	dust particle
w	=	wall

Introduction

THE structure and composition of the Martian atmosphere has been well characterized[1,2] and consists primarily of CO_2, N_2, and Ar. One of the unique aspects of designing a spacecraft that will enter the Martian atmosphere is the need to account for the presence of dust. Small dust particles are present even under quiescent conditions, and the level of dust significantly increases when a major dust storm occurs.[3] During or after a dust storm, the dust can extend to altitudes as high as 50 km.

Received 2 April 1999; revision received 2 April 2000; accepted for publication 19 May 2000.

*Aerospace Engineer, Reacting Flow Environments Branch. Associate Fellow AIAA.
†Aerospace Engineer, Thermal Protection Branch.
‡Senior Research Scientist, Reacting Flow Environments Branch. Member AIAA.
§Senior Consultant, Reacting Flow Environments Branch. Associate Fellow AIAA.

Major global dust storms occur on the average of once every 3–4 Earth years.[3] They do not, however, happen at regular intervals. There have been at least six global dust storms in the period between 1956 and 1982, but two occurred in 1977.[4,5] The concentration of dust in the atmosphere can be estimated by measuring the absorption of solar radiation. Based on measurements taken by the Viking landers during the 1977 dust storms and estimations of the strength of the vertical winds in the Martian atmosphere, it was determined that the residence time of the larger (5–10-μm diam) particles in the upper atmosphere was between 20 and 50 days after the beginning of a major dust storm.[3]

It is the larger dust particles that cause most of the erosion damage. The estimation of the residence time of the larger dust particles after the beginning of a major dust storm means the probability of an atmospheric entry vehicle encountering large dust particles while at a velocity high enough to cause erosion of the heat shield is about 2–4% (Ref. 3). This probability is high enough to warrant an analysis of magnitude of this erosion.

Information about the properties of the dust particles suspended in the Martian atmosphere after a dust storm was obtained from both orbiter and lander imaging instruments from the two Viking missions. Further details of the nature and conclusions of these measurements can be found in Ref. 3. Two pieces of information pertinent to this study are the dust particles' size distribution and composition.

The size distribution of the dust particles was inferred from solar opacity measurements on the Martian surface and infrared interferometric spectrometers aboard the orbiter vehicle on the Mariner 9 and Viking mission.[3] Based on the Mariner 9 data, a modified gamma function representing the particle size distribution was proposed with the following form[6]:

$$N(r) = Cr_p^2 \exp\left[-4\sqrt{r_p/rm}\right] \tag{1}$$

Using Eq. (1) and a value of the mode radius r_m of $0.4e{-}6$ m, we can compute a mass-averaged size distribution. The mean-mass particle diameter is 5 mm. This value for the mean-mass particle diameter is the same as the value deduced from the ground- and space-based measurements.[6]

The dust particle shape was also deduced from the measurements to be platelike. To account for a random plate orientation and to simplify their analysis, Papadopoulos et al.[3] assumed a spherical dust particle shape. This assumption will also be used in this work. From the previously described ground- and space-based measurements,[6] it was also possible to determine that the dust particles were claylike, composed primarily of SiO_2 (~70%) and Al_2O_3 (15–20%).

The dust particles move through the shock layer with a velocity that is different from that of the local flowfield. Papadopoulos et al.[3]

developed a methodology for tracking the trajectory of the dust particles from the shock wave to the vehicle surface. A brief overview of this methodology will be presented here. They assumed that the dust particles had a negligible effect on the shock layer flowfield permitting the decoupling of the fluid dynamic and dust particle trajectory computations. They based this assumption on the low mass mixing ratio (1.0$e-4$) used in their analysis.

Similar to the gas surrounding it, the motion of a dust particle is governed by the conservation of mass, momentum, and energy. With regards to the conservation of momentum, the equation of motion for a spherical particle in the shock layer is given by[3]

$$\frac{\mathrm{d}V_p}{\mathrm{d}t} = \frac{3}{8}\left[\frac{\rho}{\rho_p}\right]\left[\frac{C_D}{r_p}\right](\Delta V)^2 \tag{2}$$

The drag coefficient used in Eq. (2) comes from an expression that was developed for spheres in continuum and rarefied flows.[7] The relation includes the effect of temperature difference between the dust particle and the surrounding gas. At a relative Mach number of 3.5, the drag coefficient of a dust particle varies between 1.7 and 2.4 over particle Reynolds numbers ranging from 10 to 0.1 (Ref. 3).

When a dust particle enters the shock layer, its surface heats up rapidly. If the sublimation temperature is reached, the particle surface will begin to vaporize and the particle size will decrease. This is an important effect because the damage a particle does to the heatshield is a function of its kinetic energy. Neglecting this effect overestimates the damage that will take place. The system of equations used in Ref. 3 includes expressions to compute the particle surface temperature and the reduction of particle radius that may take place.

Once a dust particle reaches the heatshield surface with a certain velocity, size, and impact angle, an analysis is performed to determine that amount of damage that it will do to the heatshield. The methodology developed in Ref. 3 to compute the impact damage is an approximate one because the determination of cratering of surfaces subjected to hypervelocity impact is a complex physical problem. Many factors influence the extent of cratering including particle kinetic energy, the shape and size of the particle, and the composition, density, and strength of both the particle and the heatshield.

During the Apollo project, experiments were performed to determine the craters caused when spherical projectiles were fired into a glass slab. The projectile diameters ranged from 0.4 to 1.6 mm with velocities ranging from 0.25 to 7 km/s (Ref. 8). Based on the experimental results, an empirical curve fit to the data was developed based on the assumption that the crater diameter is proportional to the kinetic energy of the impacting projectile to the one-third power. For a glass heatshield, an example of which would be a space shuttle FRCI-12 tile, the ratios of crater diameter and depth to the projectile radius are given by

$$d_c/d_p = 0.113V_p^{0.667} \tag{3}$$

$$y/d_p = 0.3016d_p^{0.4}V_p^{0.667} \tag{4}$$

The particle velocity V_p is in units of meters per second. Similar relations were developed by Kessler and Su[9] for use with a virgin AVCOAT ablator material, such as was used on the space shuttle. Papadopoulos et al.[3] modified these relations somewhat to account for the greater damage that will occur to the low-density charred surface that will be present if the material is ablating and arrived at the following expressions:

$$d_c/d_p = 0.048V_p^{0.667} \tag{5}$$

$$y/d_p = 0.024V_p^{0.667} \tag{6}$$

To compute the overall erosion of the heatshield over time, these expressions are used in conjunction with the size and velocity of all dust particles that impact the vehicle surface. The equation to compute the total erosion is[3]

$$y_{\text{total}} = d_c^2 yN\cos(\theta) \tag{7}$$

The cosine term is used as a geometric factor for multiple, sequential impacts. For the shallow craters that are caused by impacts with a glass surface, $\theta = 0$. For the assumed hemispherical shape caused by impact with an ablative material, $\theta = 45$. The total number of particles per unit area that impact the surface is given by the expression

$$N = \int \frac{\rho_\infty M_r}{\sum m_p}\,\mathrm{d}s \tag{8}$$

In Ref. 3, the dust erosion analysis methodology was applied to a 26-m, 70-deg half-angle cone entering the Martian atmosphere at 8.6 km/s. The vehicle was traveling along an aerocapture trajectory close to the overshoot boundary. The vehicle reaches a minimum altitude of 41 km and is below 60-km altitude for about 400 s. The vehicle had a maximum L/D of 0.3 with a ballistic coefficient of 200 kg/m^2.

Two different forebody heatshield materials were analyzed, space shuttle ceramic tiles, which have a glassy surface, and AVCOAT-5026, which is an ablative heatshield material.

The analysis presented in Ref. 3 was based on certain assumptions. One of the assumptions made was that dust mass mixing ratio, the ratio of dust mass to ambient atmospheric mass, had a constant value of 1.0$e-4$ throughout the Marian atmosphere. This implies that for the period of increased dust activity during and after a global dust storm the dust is uniformly mixed within the atmosphere. Another assumption that was made was that an axisymmetric flow computation would provide an adequate description of the flow around the vehicle.

The results for this vehicle were that the ceramic tile thermal protection system (TPS) would suffer a peak erosion near the stagnation line of 9.7 mm. The erosion level decreased with increasing radial distance away from the stagnation point. The ablating TPS experienced a higher peak level of erosion, about 10.2 mm. The amount of erosion was a function of the vehicle's ballistic coefficient. A vehicle using the ceramic TPS with a ballistic coefficient of 300 kg/m^2 had a stagnation point dust erosion value of 14.3 mm. When the ballistic coefficient was reduced to 100 kg/m^2, the erosion decreased to 4.8 mm.

The levels of surface erosion due to dust were quite significant. If the AVCOAT TPS was used, an additional 1900 kg of material had to be added to counter the expected level of surface erosion. This amounted to 29% of the total TPS mass. Clearly, in the age of faster–better–cheaper planetary missions this amount could have an adverse impact on mission scope and feasibility.

The purpose of this paper is to determine whether the results obtained by Papadopoulos et al.[3] were representative for all Mars missions or if perhaps they were more of a worst-case scenario. Using the methodology described in the first part of this paper, the heatshield erosion caused by dust was computed for the Mars 2001 Lander vehicle. Several of the assumptions used in Ref. 3 were removed. The current analysis uses three-dimensional computational fluid dynamics (CFD) solutions to characterize the flowfield around the vehicle and uses a sophisticated Mars atmospheric model to determine the mass mixing ratio as a function of altitude.

Mars 2001 Lander Vehicle

The Mars 2001 Lander vehicle is shown in Fig. 1. Its forebody is a 70-deg half-angle cone with a nose radius of 0.6 m. The maximum vehicle diameter is 2.64 m. The afterbody is also a blunted cone with a cruise stage ring dividing the afterbody into two segments. The afterbody cone angle in front of the cruise ring is 43.4 deg, and aft of the cruise ring, the angle is 42.7 deg. The overall vehicle length is 1.63 m.

The thermal protection material used on the Mars 2001 Lander vehicle is SLA-561V. This is the same material that was used on the Mars Pathfinder lander vehicle. SLA-561V is an ablative, single-use material made from silicone resin, phenolic microballoons, silica, and cork. Because it is an ablative material, the dust erosion relations developed for the AVCOAT ablator will be applied to the SLA-561V.

Computation Points and Freestream Conditions

The Mars 2001 Lander trajectory is shown in Fig. 2. Computations that were used to provide inputs to the dust erosion analysis were

Table 1 Freestream conditions

Time, s	Altitude, km	Velocity, m/s	Density, kg/m^3	Temperature, K
30	62.3	6547.2	5.4070e−5	147.3
38	51.4	6278.5	1.9568e−4	156.6
44	44.1	6136.3	4.0276e−4	162.9
48	39.7	5362.7	6.0538e−4	166.7
60	29.5	3592.5	1.5492e−3	175.7
80	20.3	1574.0	3.4965e−3	187.9

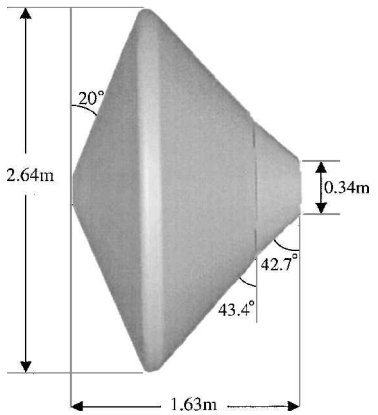

Fig. 1 Mars 2001 Lander geometry.

performed at six points along the trajectory. The points were chosen to characterize the shape of the expected stagnation point heating rate profile. The conditions at the six CFD points are shown in Table 1. Interpolation was used to obtain the flow conditions at times between the CFD points.

In regard to the Lander trajectory, note the relatively short time the vehicle surface is exposed to dust. The vehicle descends from 60 to 20 km in less than 60 s. This duration is in contrast to a vehicle flying an aerocapture trajectory that might be exposed to dust erosion for over 400 s (Ref. 3).

Improved Atmospheric Dust Model

An attempt was made to use a more sophisticated atmospheric model than simply assuming a constant dust mass mixing ratio of 1.0e−4. The atmospheric conditions at the time of vehicle entry were obtained from the Mars Global Circulation Model developed at NASA Ames Research Center.[10] The particle size distribution is computed using a modified gamma function. The coupled computational model includes seasonally dependent global circulation, dust entrainment, and settling rates. The results of the dust environment calculations consist of tables of dust particle sizes and number densities as a function of altitude and the resulting atmospheric opacity at different planetary locations and times. Dust-modified atmospheric temperature and density variations with altitude are also provided. For the computations presented in this study an opacity of 2.51 is used.

The resulting dust mass mixing ratio as a function of altitude at the time of the Mars 2001 Lander entry is shown in Fig. 3. The mass mixing ratio is negligible above 50 km. It increases with decreasing altitude. At 20 km, the ratio is still quite low, reaching a value of 3.5e−5. The peak value is only 35% the value assumed throughout the entire atmosphere in Ref. 3. The mass fraction of particles as a function of particle diameter at the 37.7-km trajectory point is shown in Fig. 4. The particles are small, with the most common particle diameter being 2.25 μm. Only 10% of the particles have a diameter of 5 μm or larger. In the atmospheric model used in Ref. 3, the greatest mass fraction was for 5-μm particles, and 7- and 9-μm particles each had mass fractions greater than 10%.

Three-Dimensional CFD Flow Solver

The flow solutions are computed using the GASP version 3 Navier–Stokes flow solver.[11] GASP is an established commercial code that has been applied to a wide array of internal and external flow problems[12–15] and has been applied to solving flows over Mars

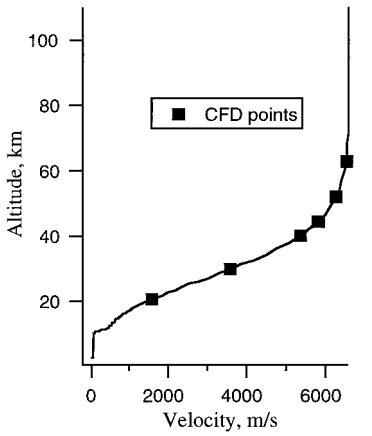

Altitude vs velocity

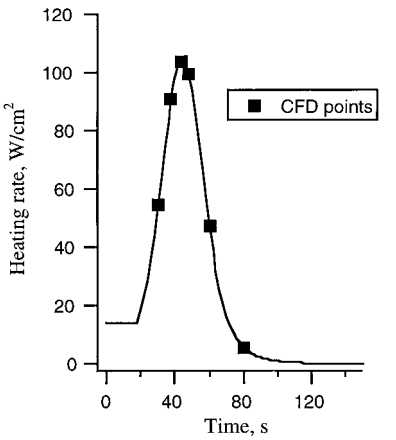

Stagnation point heating rate vs time

Fig. 2 Mars 2001 Lander trajectory.

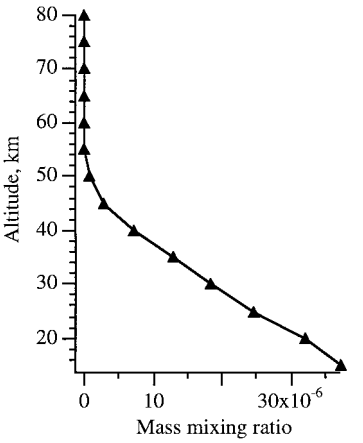

Fig. 3 Dust mass mixing ratio.

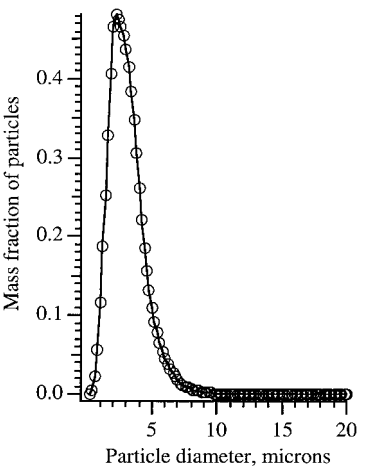

Fig. 4 Dust particle mass fraction as a function of particle size; 37.7 km.

entry mission vehicles.[16] The chemical kinetics and surface thermochemistry models available in GASP are similar to those used in previous analysis of the Mars Pathfinder vehicle.[17] GASP solves the full Navier–Stokes equations that model the conservation of density, momentum, and energy. Third-order spatially accurate Van Leer flux vector splitting[11] is used to difference the inviscid fluxes. Viscous terms are evaluated in all coordinate directions.

An eight-species, chemical nonequilibrium gas model is used. The species considered are [CO_2, CO, N_2, O_2, NO, C, N, O]. The 47 reaction kinetics model of Mitcheltree and Gnoffo[18] is used to model finite-rate chemical reactions. The species specific heats and enthalpies are obtained by assuming thermal equilibrium and using equilibrium statistical thermodynamics. Species viscosity is obtained using Blottner et al. curve fits.[19] Mixture laminar viscosity is computed using Wilke's mixing rule.[20] Species thermal conductivity is calculated using Eucken's relation (see Ref. 21). Mixture thermal conductivity is obtained using Wilke's mixing rule.[20] Species diffusion is assumed to be binary. The diffusion coefficients are obtained by assuming a constant Schmidt number of 0.8.

The surface temperature is computed by solving an energy balance at the vehicle surface[14]:

$$\kappa\frac{\partial T}{\partial \eta} + \sum_{s=1}^{\text{nspc}} \rho D h_s \frac{\partial Z_s}{\partial \eta} = \sigma \varepsilon T_w^4 + q_{\text{cond}} \tag{9}$$

The emissivity of SLA-561V ranges from 0.7 for virgin material to 0.90 for char. For the calculations presented in this study, a constant emissivity of 0.85 is applied to the entire configuration. Conduction into the vehicle surface is not modeled in the CFD computations, and so the q_{cond} term is set to zero.

The surface thermochemisty model used in this study assumes only CO_2 recombines on the surface by way of the following reactions[18]:

$$O + [s] \rightarrow O_s$$

$$CO + O_s \rightarrow CO_2 + [s]$$

$$CO + [s] \rightarrow CO_s$$

$$O + CO_s \rightarrow CO_2 + [s]$$

In the preceding reactions, $[s]$ is an available absorption site on the surface.

Grid Generation

The grid used to compute the CFD solutions covered the forebody and shoulder regions of the vehicle. To avoid using a singular line, the grid was made up of two zones. The first zone is a 61 ×25 ×65 grid that wraps around the body from the windward trailing edge across the forebody to the leeward trailing edge. The second grid is a 7 ×49 ×65 grid that models the side of the vehicle. The advantage of this type of grid topology is that it eliminates the forebody singular axis. The grids used a hyperbolic tangent distribution of normal points with a first grid spacing, normal to the wall, of 2.0e−6 m.

Grid Sensitivity and Solution Convergence

Each of the solutions presented in this study was run until an acceptable level of convergence was reached. This was evaluated in two ways. The first was to look at the L2 norm of the density residual. The solution process was continued until at least a four-order magnitude drop in the residual was achieved. A typical residual history is shown in Fig. 5a. The residual, in this case for the 48-s trajectory point computation, shows some initial instability but ultimately drops approximately five orders of magnitude.

The second method used to evaluate the solution convergence was to track the surface heating rate profile on the vehicle forebody. Heating rate is a fourth-order function of radiative equlibrium wall temperature and is a good test of solution convergence. A heating rate history along the vehicle symmetry plane for the 48-s trajectory point CFD computation is shown in Fig. 5b. The stagnation region took the longest to achieve a steady state generally requiring around 4000 iterations to do so.

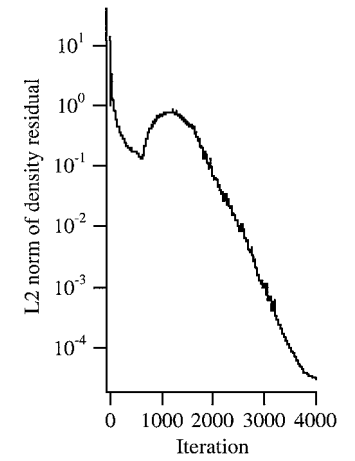

a) Residual history

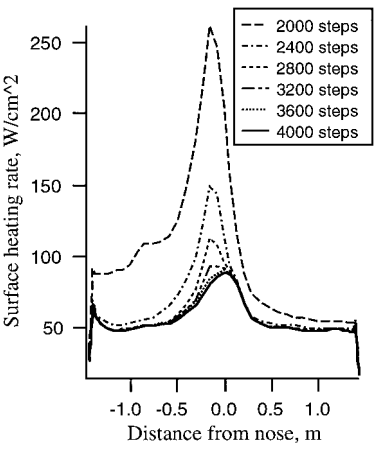

b) Surface heating rate history

Fig. 5 Convergence evaluation: 48-s trajectory point computation.

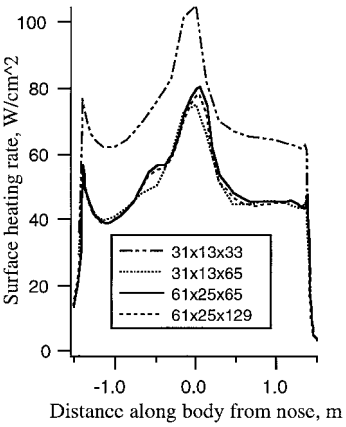

Fig. 6 Grid sensitivity study; surface heating profiles at the 38-s trajectory point.

An effort was made to determine whether the grid being used would produce a grid-independent solution. Four solutions at the 38-s freestream condition were computed. The first solution used the nominal 61 ×25 ×65 and 7 ×49 ×65 grids. The second solutions used a grid that had half as many points in the normal direction. This grid had a first grid spacing of 4.0e−6 m. The third solution used a grid with half as many points in all three directions. The final solution used a grid with twice as many points in the normal direction. This grid used a first grid spacing of 1.0e−6 m.

Figure 6 shows the resulting surface heating rate profiles along the symmetry plane. The legend only indicates the wrap-around grid dimensions for clarity. A substantial difference in the computed heating rate profile is seen when the number of points in the normal

direction is increased from 33 to 65. A much smaller change is seen when the number of streamwise and circumferential points is doubled (the nominal grid) while keeping the number of normal points at 65. When the number of normal grid points is increased from 65 to 129, there is a small difference in the computed heating rate, primarily in the stagnation region. The maximum difference between the 65 and 129 normal grid point solutions is 4%. This small difference did not justify doubling the computer requirements and so the 61 ×25 ×65 and 7 ×49 ×65 grids were used for all solutions in this study.

CFD Results: Stagnation Line Temperature Profiles

The CFD solutions provide velocity field, temperature, and pressure data for the dust erosion analysis. Interpolation is used to obtain data between the CFD points. Figure 7 shows stagnation line temperature profiles for the six CFD points. Figure 7 also shows the change in the shock standoff distance that occurs as the vehicle descends through the atmosphere. The shock moves closer to the body during the initial part of the descent, up to at least the 48-s point. Then as the velocity decreases more rapidly the shock location moves out. When the shock moves closer, the dust particles have less space to decelerate and sublimate. The reverse is true when the shock location moves out.

The sublimation temperature of silicon dioxide, the primary constituent of Martian dust, will range from 2600 to 2700 K for the pressures expected during the Mars 2001 Lander descent. The dust particles heat up rapidly once they enter the shock layer and will experience sublimation at least until the 60-s point in the trajectory. Sublimation reduces the size of the particles and, therefore, the damage they will cause.

Heatshield Recession Due to Dust Erosion

The various inputs were fed to the dust erosion code, and the integrated surface erosion was computed for the Mars Lander 2001 vehicle. Figure 8 shows the surface recession rate at the stagnation point as a function of time. The surface recession is a function of the kinetic energy of the impacting dust particles. The mass mixing ratio increases with decreasing altitude, but the particle velocity decreases. The kinetic energy of an impacting particle of constant size is an order of magnitude less at 20 km than it is at 37.7 km. The peak recession rate occurs at 55 s and corresponds closely to the time where the peak dynamic pressure point occurs.

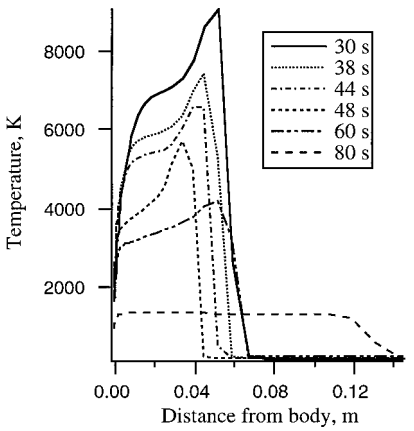

Fig. 7 Stagnation line temperature profile.

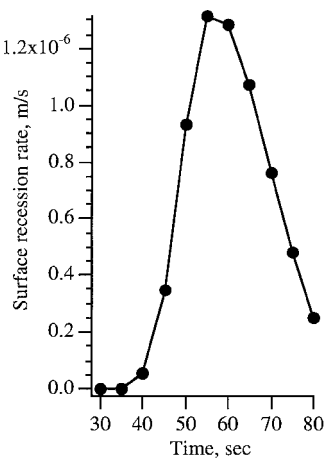

Fig. 8 Dust erosion rate at the stagnation point.

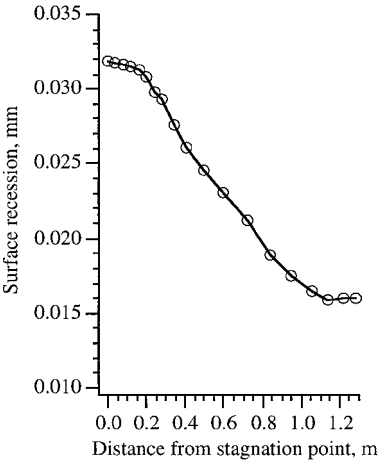

Fig. 9 Total surface recession: windward symmetry plane.

The total recession is obtained by integrating the recession rate curves over the entire forebody. Figure 9 shows the total recession on the windward symmetry plane. The windward symmetry plane is where the maximum recession occurs. The maximum recession is seen at the stagnation point and is 0.032 mm. The amount of recession decreases away from the stagnation point. At the vehicle shoulder the rate is less than one-half the stagnation point value.

The computed dust erosion for the Mars 2001 Lander vehicle is significantly less than for the aerocapture vehicle analyzed in Ref. 3. The aerocapture vehicle experienced dust erosion levels in the 1–10 mm range. The reasons for this can be attributed to the different types of entry trajectory and the different atmospheric dust models used in the two analyses. The aerocapture vehicle had a much longer exposure time to the dust particles. More recent atmospheric dust models indicate a more benign situation than was previously assumed. The largest mass fraction in the dust environment used in Ref. 3 was for particle diameters of 5.5 μm. Particles of this diameter have an order of magnitude greater mass than the 2.25-μm particles that are at the peak of the distribution curve used in this study. In addition, Ref. 3 used a constant mass mixing ratio of $1.0e-4$. In this study, the mixing ratio varied strongly with altitude and never exceeded $3.5e-5$. The larger diameter particles and larger, constant mass mixing ratio assumptions were excessively conservative in view of the more precise atmospheric dust model used in this study and led to larger TPS surface recession predictions.

Conclusions

Based on the results presented, it would appear that heatshield surface recession on the Mars 2001 Lander vehicle due to dust erosion is not as significant as earlier studies had suggested. More recent atmospheric dust models indicate that the most prevalent dust particles are smaller and that the dust mass mixing ratio is less than was previously believed. For the Mars 2001 Lander vehicle analyzed, dust erosion was found to be insignificant. Admittedly, this result is for a specific vehicle flying a specific trajectory at a specific point in time. An aerocapture vehicle, which will experience a longer exposure time, would experience a greater level of dust erosion, and there are still uncertainties in the dust mass mixing ratio and particle size distribution models. The techniques presented can be applied to any Mars entry vehicle and should be used as part of the TPS design process.

References

[1]Seiff, A., and Kirk, D. B., "Structure of the Atmosphere of Mars in Summer at Mid-Latitudes," *Journal of Geophysical Research*, Vol. 82, No. 8, 1977, pp. 4364–4378.

[2]Owen, T., Biemann, K., Rushneck, D. R., Biller, J. E., Howarth, D. W., and LaFleur, A. L., "The Composition of the Atmosphere at the Surface of Mars," *Journal of Geophysical Research*, Vol. 82, No. 8, 1977, pp. 4633–4639.

[3]Papadopoulos, P., Tauber, M., and Chang, I.-D., "Heat Shield Erosion in a Dusty Martian Atmosphere," *Journal of Spacecraft and Rockets*, Vol. 30, No. 2, 1993, pp. 140–151.

[4]Haberle, R. M., "Interannual Variability of Global Dust Storms on Mars," Science, Vol. 234, Oct. 1986, pp. 459–461.

[5]Zurek, R. W., "Martian Great Dust Storms: An Update," Icarus, *International Journal of the Solar System*, Vol. 50, No. 2, 1982, pp. 288–310.

[6]Toon, O. W., Pollack, J. B., and Sagan, C., "Physical Properties of the Particles Composing the Martian Dust Storm of 1971–1972," *Icarus*, Vol. 30, No. 5, 1977, pp. 663–696.

[7]Henderson, C. B., "Drag Coefficients of Spheres in Continuum and Rarefied Flows," *AIAA Journal*, Vol. 14, No. 6, 1976, pp. 1477–1499.

[8]Flaherty, R., "Impact Characteristics in Fused Silica," OART Meteoroid Impact Penetration Workshop, Manned Spacecraft Center, Houston, TX, Oct. 1968.

[9]Kessler, D. J., and Su, S. Y., "Hypervelocity Impact Investigation and Meteoroid Shielding Experience Related to Apollo and Skylab," NASA CP 2360, pp. 247–274.

[10]Murphy, J., Pollack, J., Haberle, R., Leovy, C., Toon, O., and Schaeffer, J., "Three-Dimensional Numerical Simulation of Martian Global Dust Storms," *Journal of Geophysical Research*, Vol. 100, No. B12, 1995, pp. 26,357–26,376.

[11]Walters, R. W., Slack, D. C., Cinnella, P., Aplebaum, M., and Frost, C., "A User's Guide to GASP," Virginia Polytechnic Inst. and State Univ., Research Rept. NASA Grants NAG-1-766 and NAG-1-1045, Blacksburg, VA, Nov. 1990.

[12]Gnoffo, P., Weilmuenster, K., and Alter, S., "Multiblock Analysis for Shuttle Orbiter Re-Entry Heating from Mach 24 to Mach 12," *Journal of Spacecraft and Rockets*, Vol. 31, No. 3, 1994, pp. 367–377.

[13]Olynick, D. R., and Tam, T., "Trajectory Based Validation of the Shuttle Heating Environment," AIAA Paper 96-1891, June 1996.

[14]Olynick, D. R., and Henline, W. D., "Numerical Benchmarks for Navier–Stokes Heating Calculations on Access to Space Vehicles," AIAA Paper 95-2078, June 1995.

[15]Palmer, G., Henline, W. D., Olynick, D. R., and Milos, F. S., "A Heating Analysis and Thermal Protection System Sizing of a Lifting Body Single-Stage-to-Orbit Vehicle," AIAA Paper 95-2080, June 1995.

[16]Papadopoulos, P., Venkatapathy, E., Henline, W. D., and Wercinski, P., "Aerothermal Heating Simulations with Surface Catalysis for the Mars 2001 Aerocapture Mission," AIAA Paper 97-0473, Jan. 1997.

[17]Gupta, R., and Lee, K., "An Aerothermal Study of MESUR Pathfinder Aeroshell," AIAA Paper 94-2025, June 1994.

[18]Mitcheltree, R. A., and Gnoffo, P. A., "Wake Flow About a MESUR Mars Entry Vehicle," AIAA Paper 94-1598, June 1994.

[19]Blottner, F. G., Johnson, M., and Ellis, M., "Chemically Reacting Viscous Flow Program for Multi-Component Gas Mixtures," Sandia National Lab., Rept. SC-RR-70-754, Albuquerque, NM, 1971.

[20]Wilke, C. R., "A Viscous Equation for Gas Mixtures," *Journal of Computational Physics*, Vol. 18, No. 4, 1950, pp. 517–519.

[21]Vincenti, W. G., and Kruger, C. H., *Introduction to Physical Gas Dynamics*, Krieger, Malabar, FL, 1965, p. 21.

T. C. Lin
Associate Editor